# Optimization designed large-stroke MEMS micromirror for adaptive optics

**Quan Sun (孙 全)[1*], Kelly He[2], and Edmond Cretu[2]**

[1] *College of Optoelectronics Science and Engineering, National University of Defense Technology, Changsha 410073, China*

[2] *Department of Electrical and Computer Engineering, University of British Columbia, 2332 Main Mall, Vancouver, V6T1Z4, Canada*

[*] *E-mail: sunquan.nudt@gmail.com*

Received May 25, 2010

A novel micromirror based on the PolyMUMPs process is designed and presented. The hexagonal micromirror with a diameter of 450 $\mu$m consists of three supporting bilayer cantilevers and a mirror plate. The bilayer cantilevers, formed with a polysilicon layer and a gold layer, elevate the mirror plate according to residual stress-induced bending. Both analytical and finite element analysis (FEA) models are built to calculate the elevated height of the free end of the cantilever. The analytical solution is in accordance with the FEA simulation results, with longitudinal stresses applied only. Results of a three-dimensional (3D) simulation with two direction stresses applied also show the elevated height to be proportional to the width of the cantilever and the length of the gold layer. Due to the torque of the joint, the elevated heights of the two kinds of cantilevers assembled with the mirror plates are much smaller than those of the free end of the cantilevers. Both micromirrors with different cantilevers are fabricated. The elevated heights of the fabricated micromirrors are measured using Veeco optical profiler, which show good coincidence with simulation results.

*OCIS codes:* 220.4000, 230.3990, 230.4685.

*doi: 10.3788/COL20100812.1163.*

Recently, microelectromechanical system (MEMS) based micromirror arrays have received much attention. They have been applied in a wide range of areas, such as optical switches[1,2] and displays[3,4], high-performance imaging including astronomy imaging and biomedical imaging[5−7], and laser-based communication[8,9]. MEMS-based micromirrors have high operating speed, low mass, low cost, and can be integrated with electronics through batch micro-fabrication processes. A successful micromirror design must establish a trade-off between multiple competing considerations, such as mirror surface quality, scan angle, fill factor, surface area, actuation speed, and cost. The final parameters of a micromirror design depend on its intended application and the employed fabrication process. In this letter, we discuss a new set of micromirror designs and investigate its fabrication using a standard foundry process: MEMSCAP's PolyMUMPs process. This standard commercial process is mature, with a low cost and short fabrication cycle. The micromirror structure is supported by three stress-induced flexure cantilevers and controlled by three electrodes that exhibit a large stroke and tip/tilt/piston motion.

PolyMUMPs is a three-layer polysilicon surface micromachining process. The thickness and typical stress of the layers are summarized in Table 1[10]. The polysilicon layers Poly1 and Poly2 are commonly used as structural materials, whereas Poly0 layer is generally used as electrical interconnections. Deposited oxide layers Oxide1 and Oxide2 are used as the two sacrificial layers, whereas a silicon nitride layer is used as an electrical insulation between polysilicon and substrate. The final deposited layer is a metal layer (Gold) used for various functions, from defining bond pads and electrical routing to forming highly reflective mirror surfaces. Oxide1 is usually etched to generate the gap between actuators and electrodes after the structure is released.

Considering the pull-in effect, a 2-$\mu$m gap is not enough to be an adequate stroke. One method of increasing the gap is to exploit the residual stress difference between the polysilicon layer and the metal layer to create curved structures that lift off the substrate when deliberately undercut by an etchant[11]. Our micromirror prototype is designed to use this effect to form supporting cantilevers, which bend upward to elevate the mirror plate as polysilicon has a small compressive residual stress, whereas the gold film has a large tensile residual stress. However, this stress-induced curve also has a harmful effect on the mirror surface flatness. Although annealing can lower internal stresses, the difference between the two layer stresses is still high to cause the bowing of the

**Table 1. Mechanical Parameters of the PolyMUMPs Process Layers**

| Film | Thickness ($\mu$m) | Typical Stress (MPa) |
|---|---|---|
| Nitride | 0.6 | 90 |
| Poly0 | 0.5 | –25 |
| Oxide1 | 2 | – |
| Poly1 | 2 | –10 |
| Oxide2 | 0.75 | – |
| Poly2 | 1.5 | –10 |
| Metal (Gold) | 0.5 | 50 |

 

mirror surface. One effective way to decrease bowing is to make the released mirror plate as thick as possible. The typical method in a PolyMUMPs process is to stack Poly1 and Poly2 with a trapped layer of Oxide2 between them[12].

The design of the micromirror depicted in Fig. 1 was made up of a hexagonal mirror plate and three V-shaped supporting cantilevers. The diameter of the mirror plate is 380 $\mu$m. As shown in Fig. 1(a), each cantilever was fixed to an anchor on one side and connected to the mirror plate with an improved joint on the other side. The cantilevers were fabricated using Poly2 (the thinnest layer) and Gold, which could generate the largest curvature[13] to elevate the mirror plate, as shown in Fig. 1(b). The mirror plate was designed with four layers, where Oxide2 was trapped and preserved between Poly1 and Poly2 by sealing all edges of Oxide2 (mirror perimeter and all release hole perimeters); Gold was deposited on top. There were also 88 release holes in 2-$\mu$m size passing through the mirror plate to ensure that the Oxide1 layer was fully etched away within the standard release time. The three rhombuses, as shown in Fig. 1(a), were three electrodes fabricated by Poly0 under the mirror plate. Each electrode was wired to a separated bond pad, which provided independent actuation voltages. If one or two electrodes were biased, the mirror would tilt relative to the horizontal plane; whereas if all three were applied with an equal voltage, the mirror would move up and down. When the voltages were removed, the mirror plate was lifted up to its original level by the restoring force of the cantilevers.

The lift-off height of the cantilever depends on its design factors, including the deposition area of gold and the width of the cantilever. In the following, we will discuss the optimization designs to reach the largest lift-off height.

The two designed structures of the cantilever are illustrated in Fig. 2. The structures were made of Poly2 and Gold. The first design (denoted as Design I) had gold film deposited only on the first half of the cantilever, whereas the second design (denoted as Design II) had gold film deposited on the entire cantilever. Both designs had the same geometry, consisting of two 195-$\mu$m-long beams. Poly2 should enclose 3 $\mu$m of Gold on each side according to the design rules of PolyMUMPs[10]. An analytical solution was conducted on a rectangular cantilever to estimate the tip deflection of the bilayer beam[14]. We used this analytical solution to calculate the lift-off height of the Design I cantilever and compared it with that obtained by finite element analysis (FEA).

From the equilibrium boundary conditions of internal forces and the strain at the interface of the two layers, we can derive an approximation for the radius of curvature $R$ and tip deflection $h$ in terms of residual stress when the widths of the two layers are not equal:

$$R = \frac{\left(w_1 E_1 h_1^2\right)^2 + \left(w_2 E_2 h_2^2\right)^2 + 2 w_1 w_2 E_1 E_2 h_1 h_2 \left(2h_1^2 + 3h_1 h_2 + 2h_2^2\right)}{6 w_1 w_2 E_1 E_2 h_1 h_2 \left(h_1 + h_2\right)\left(\frac{\sigma_2}{E_2} - \frac{\sigma_1}{E_1}\right)}, \tag{1}$$

$$h = R\left[1 - \cos\left(\frac{L}{R}\right)\right], \tag{2}$$

where $h_1$ and $h_2$ are the thicknesses of the polysilicon and the gold layers, respectively; $L$ and $w_n$ are the $(n = 1,2)$ length and widths of the beams, respectively; $E_n$ and $I_n (n = 1, 2)$ are the Young's moduli and the moments of inertia, respectively; $\sigma_n (n = 1, 2)$ are the residual stresses of materials.

We divided the cantilever into two parts, namely, one curved bilayer beam and one straight polysilicon beam, and calculated the deflection of each. With one end of the bilayer beam fixed to an anchor, the other end was elevated. As the length of the bilayer beam was much larger than its width, we approximated it as a rectangle bilayer beam and used Eq. (2) to calculate the tip deflection $h$ (as shown in Fig. 3(a)). The polysilicon beam formed a 120° angle with the end of the bilayer beam and sloped in the tangent plane of the curved

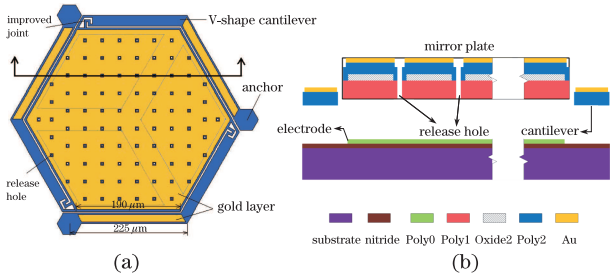


Fig. 1. Micromirror mechanical design layout (not to scale). (a) Top view of the micromirror; (b) cross-sectional view of the released micromirror.

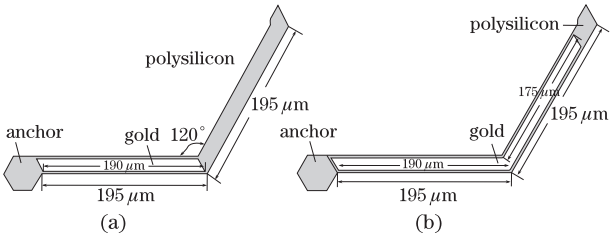


Fig. 2. Cantilever structure design diagrams. (a) First cantilever design; (b) second cantilever design.

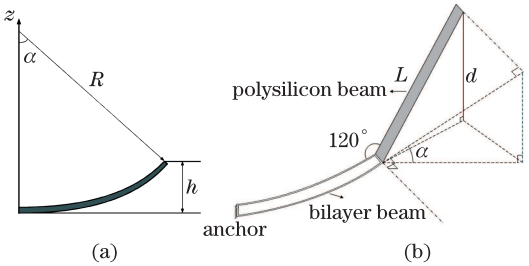


Fig. 3. Schematic drawing of the Design I model geometry. (a) Side view of the first half of the cantilever; (b) 3D geometry of the second half of the cantilever.

bilayer beam at the tip. The polysilicon beam deflection $d$ was calculated by solving the three-dimensional (3D) geometry in Fig. 3(b).

As shown in Fig. 3(a), $\alpha$ is the angle between the ground and the tangent of the first half of the cantilever at the tip. It can be approximated by $\alpha = L/R$. The amount of deflection in the second half of beam $d$ can be expressed as $d = L\sin\alpha/2$. The total lift-off height of the Design I cantilever is the sum of the tip deflections in the first and second halves of the beams.

A 3D model of the Design I cantilever was built to estimate the lift-off height in COMSOL Multiphysics program. The structure geometry was the same as that in Fig. 2(a), with a polysilicon width of 20 $\mu$m and a gold width of 14 $\mu$m. Figure 4 shows the images of the simulation results of the half and entire cantilevers, with two-dimensional (2D) residual stresses applied. Both analytical and simulation results are summarized in Table 2.

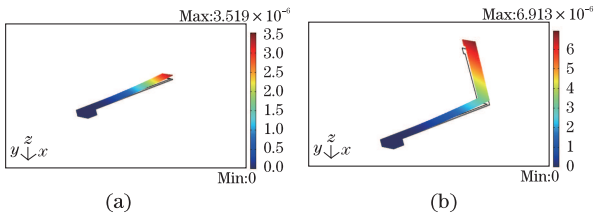


(a) (b)

Fig. 4. COMSOL simulation results with 2D stress applied on the Design I cantilever. (a) Deformation of the first half of the cantilever; (b) deformation of the entire cantilever.

**Table 2. Analytical and COMSOL Simulation Results of the Cantilever**

| Polysilicon Width: 20 $\mu$m | Analytical | COMSOL Simulation Results ($\mu$m) | |
|---|---|---|---|
| Gold Width: 14 $\mu$m | Result ($\mu$m) | 1D Stresses | 2D Stresses |
| Deflection of First Half of Cantilever | 4.868 | 4.934 | 3.519 |
| Total Deflection of Cantilever | 9.691 | 9.643 | 6.913 |

As shown in Table 2, the analytical results are very close to the simulation results when applying one-dimensional (1D) longitudinal residual stresses to the model, as the stress-induced flexure along the width's direction can be ignored. However, when 2D residual stresses are considered, the deflection values are reduced due to the transversal flexure of the cantilever and the width difference between the two layers.

The total tip deflections with different cantilever widths were also simulated. As shown in Fig. 5, with the cantilever width increasing, the total tip deflections increases. However, by increasing the cantilever width, the effective area of the mirror decreases. A trade-off must be made between them, and thus we set the cantilever width to 20 $\mu$m. All the simulations below were carried out using a 20-$\mu$m-wide cantilever.

Simulation of the Design II cantilever was also conducted in COMSOL. Figure 6 shows that the tip deflection reaches 10 $\mu$m. Compared with Fig. 4(b), the tip deflection of the cantilever increases as the deposited area of gold increases.

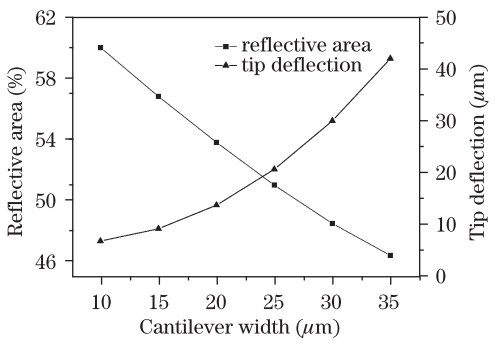


Fig. 5. Cantilever width versus effective area and tip deflection.

Micromirror models with a mirror plate assembled with two kinds of cantilevers were also built in COMSOL. The simulation results are shown in Fig. 7. In Figs. 7(a) and (b), the lift-off heights of the micromirror with the Design I and Design II cantilevers are 3.9 and 2.8 $\mu$m, respectively. These elevated heights of the mirror plate are much smaller than the tip deflections of the cantilevers. The main reason for this is the torque generated at the joint point that pulls down the mirror towards the substrate. The amount of torque is proportional to the angle between the mirror plate and the tangent plane of the cantilever at the joint point. When the pull-down effect of the torque equals the elevated forces of the cantilevers, the mirror plate is in equilibrium. To reduce this torque, an optimized joint, which consists of two 2-$\mu$m-thick springs, was designed, as shown in Fig. 1(a), which increased the elevated height by almost 10%[13]. Figures 7(c) and (d) show the enlarged images of the torsional angles at the joint point. The curved Design II cantilever causes much larger torsional angle than the straight beam of the Design I cantilever. Although the Design II cantilever has a higher deflection, it provides a lower elevated height for the mirror plate.

These micromirrors with two designs of cantilevers were fabricated using the PolyMUMPs process. Figure 8(a) shows the microscopic image of a fabricated micromirror with a Design I cantilever, whereas Fig. 8(b) shows the image of a fabricated micromirror with a Design II cantilever. The three control electrodes beneath the mirror plate are connected to the pads by three wires, and the mirror plates are connected to the ground by their anchors. The profiles of the electrodes and wires are

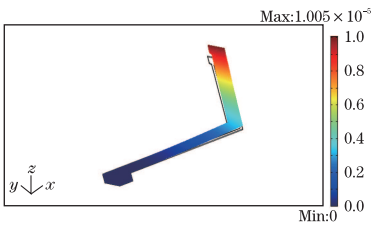


Fig. 6. COMSOL simulated deformation result of the Design II cantilever.

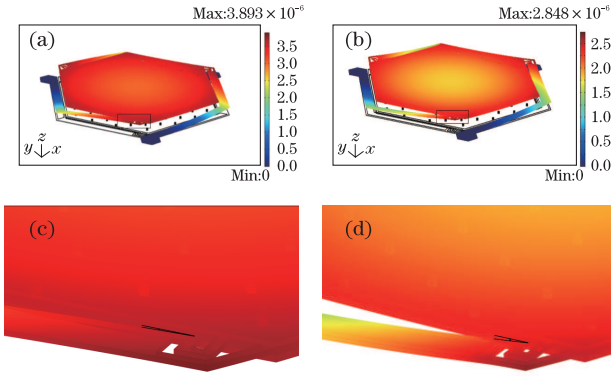


Fig. 7. COMSOL simulation results of the micromirror lift-off height. (a) Micromirror with the Design I cantilever; (b) micromirror with the Design II cantilever; (c) torsional angle of the Design I cantilever; (d) torsional angle of the Design II cantilever.

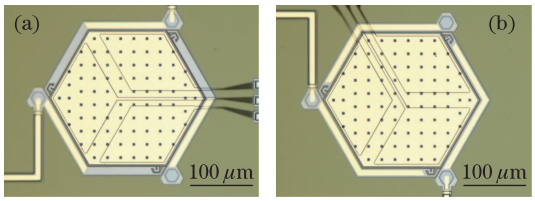


Fig. 8. Microscopic images of the fabricated micromirrors. (a) Micromirror with the Design I cantilever; (b) micromirror with the Design II cantilever.

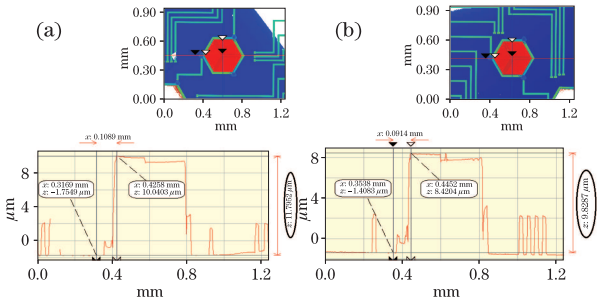


Fig. 9. Veeco optical profiler measurements of the fabricated micromirrors. (a) Micromirror with the Design I cantilever; (b) micromirror with the Design II cantilever.

observed in the mirror plate due to the print-through effect[12].

The lift-off heights of the fabri cated micromirrors were measured using a Veeco optical profiler. The measurement results are shown in Fig. 9. The straight lines in the top images show the sectional views of $x$ profile data. The distances from the top surface of the mirror plate to the substrate are 11.8 and 9.8 $\mu$m, respectively. Subtracting the 4.25-$\mu$m thickness of the mirror plate and the 2-$\mu$m thickness of the gap formed by removing Oxide1, the actual lift-off height of the micromirror is 5.55 $\mu$m with the Design I cantilever and 3.55 $\mu$m with the Design II cantilever. The measurement results show the same conclusion as the simulation results. The difference between the two values comes from the approximation of the FEA models and the test errors. As the parameters applied in FEA model are the typical values of PolyMUMPs process, the real values of stresses and thicknesses of the layers are difficult to control in the process. They vary greatly with respect to process temperature, doping level, and other fabrication parameters. We will discuss these effects in our future work.

A novel piston/tip/tilt micromirror based on PolyMUMPs process is designed and explored. Both analytical solution and FEA performed in COMSOL are illustrated to calculate the lift-off heights of the different cantilever structures. Calculations show that the analytical result is in accordance with the FEA simulation results, whereas stresses are applied longitudinally only. Simulation results also show the lift-off height of the micromirror with the Design I cantilever to be larger than that of the micromirror with the Design II cantilever, although the Design II cantilever has a higher deflection than the Design I cantilever. These two different cantilever designs of micromirrors are fabricated, and the lift-off heights of each are measured using Veeco optical profiler. The measurement results and simulation results show good coincidence.

## References

1. P. M. Hagelin, U. Krishnamoorthy, J. P. Heritage, and O. Solgaard, IEEE Photon. Technol. Lett. **12,** 882 (2000).
2. W. Li, J. Liang, X. Li, Y. Zhong, Z. Liang, and D. Sun, Acta Opt. Sin. (in Chinese) **28,** 1151 (2008).
3. M. C. Wu, Proc. SPIE **5715,** 1 (2005).
4. D. Wang and S. Wei, Acta Opt. Sin. (in Chinese) **28,** 51 (2008).
5. M. A. Michalicek, N. Clark, and J. H. Comtois, Proc. SPIE **3353,** 805 (1998).
6. S. Waldis, F. Zamkotsian, P. A. Clerc, W. Noell, M. Zickar, and N. de Rooij, IEEE J. Sel. Top. Quantum Electron. **13,** 168 (2007).
7. A. Dubra, D. C. Gray, J. I. W. Morgan, and D. R. Williams, Proc. SPIE **6888,** 688803 (2008).
8. L. M. C. A. Thompson, M. W. K. Flath, S. C. Wilks, R. A. Young, G. W. Johnson, and A. J. Ruggiero, Proc. SPIE **4821,** 129 (2002).
9. J. Li, H. Q. Chen, G. P. Yan, Y. Liu, and P. Wu, Proc. SPIE **5985,** 59851R (2005).
10. J. Carter, A. Cowen, B. Hardy, R. Mahadevan, M. Stonefield, and S. Wilcenski, *PolyMUMPs Design Handbook* (Revision 11.0, MEMSCAP Inc., 2005).
11. M. A. Rosa, D. D. Bruyker, A. R. Volkel, E. Peeters, and J. Dunec, J. Micromech. Microeng. **14,** 446 (2004).
12. J. Comtois, A. Michalicek, W. Cowan, and J. Butler, Sensors and Actuators A **78,** 54 (1999).
13. Q. Sun, M. Cai, N. Y. Wang, and E. Cretu, Proc. SPIE **7510,** 751003 (2009).
14. S. M. N. Rao, P. Pandojirao-Sunkojirao, N. Dhaubanjar, M. Chiao, and J. Chiao, Int. J. Optomechatron. **3,** 149 (2009).